

The Spherical Tokamak Fusion Power Plant

H R Wilson 1), G Voss 1), J-W Ahn 2), R J Akers 1), L Appel 1), A Bond 3), A Cairns 4), J P Christiansen, 1), G Counsell, 1), A Dnestrovskij 2,5), M Hole 1), A Kirk 1), P Knight 1), C N Lashmore-Davies 1), K G McClements 1), M O'Brien 1) and S Tsun 5)

- 1) EURATOM/UKAEA Fusion Association, Culham Science Centre, Abingdon, UK
- 2) Imperial College, London, UK
- 3) Reaction Engines Ltd, Stanford-in-the-Vale, Oxfordshire, UK
- 4) University of St Andrews, Fife, KY16 9SS UK
- 5) I V Kurchatov Institute, Moscow, Russia

e-mail contact of main author: howard.wilson@ukaea.org.uk

Abstract. The design of a 1GW(e) steady state fusion power plant, based on the spherical tokamak concept, has been further iterated towards a fully self-consistent solution taking account of plasma physics, engineering and neutronics constraints. In particular a plausible solution to exhaust handling is proposed and the steam cycle refined to further improve efficiency. The physics design takes full account of confinement, MHD stability and steady state current drive. It is proposed that such a design may offer a fusion power plant which is easy to maintain: an attractive feature for the power plants following ITER.

1. Introduction

The promising results from the pioneering spherical tokamak (ST), START, are beginning to be confirmed on the next generation of larger STs: MAST and NSTX. These include: good tokamak-like confinement, low halo current magnitude and asymmetries, high natural elongation and high β capability, all of which are attractive features for a fusion power plant. In this paper, we review the status of research on the design of an ST power plant, STPP. The base-line design described here has been developed through an iterative process, so that it self-consistently takes account of constraints imposed by thermodynamics, neutronics, economics and plasma physics. The engineering design for this device has been described elsewhere [1,2] so, as space is restricted here, we encourage the reader to consult these references for more details on that aspect of the design. In this paper we concentrate mainly on the plasma physics issues, and restrict discussion of the extensive technology and engineering research to a brief overview. In particular, we begin in Section 2 with a discussion of the plasma physics parameters associated with the base-line design and how we arrive at this choice. Then, in Section 3 we address the issue of steady state current drive, which has a large impact on the overall design. In Section 4 we describe MHD stability issues, including vertical stability and pressure-limiting instabilities. In Section 5 we describe studies of prompt losses of α particles and then, in Section 6, we address confinement and exhaust. In Section 7 we provide an overview of the engineering and technology issues we have addressed, and close in Section 8 with a summary and conclusions.

2. Base-line design

The base-line design has been developed through many iterations to satisfy the engineering and physics constraints, and converge on a self-consistent design. The plasma parameters for the design on which we base the study of this report are given in Table 1. The starting point is a desire to develop a 1GW(e) power plant (corresponding to ~ 3 GW fusion power) which then allows a comparison with other, similar power output, devices. All other device parameters are then derived as follows. An aspect ratio of 1.4 is chosen, which is close to the optimum found in parameter scans using systems codes (in terms of cost of electricity); this also provides a complementary design to that of the ARIES team, which selected $A=1.6$ as the

Parameter	Value
Major radius/minor radius (m)	3.42/2.44
Elongation	3.2
Triangularity	0.55
Plasma current (MA)	31
Centre rod current (MA)	30.2
Safety factor on axis, at edge	3, 15
Line-avge, central density ($\times 10^{19} \text{m}^{-3}$)	10.8, 12.6
Greenwald density ($\times 10^{19} \text{m}^{-3}$)	16.6
Average temperature (keV)	22
$\beta(\%)$, β_N	59, 8.2
Internal inductance, $l_i(2)$	0.21
Z_{eff}	1.6
Fusion power (GW)	3.1
CD power (MW)	50
Auxiliary CD (MA)	2.3
Pressure driven current (MA)	28.7
Confinement $H_{\text{IPB98}(y,1)}$, $H_{\text{IPB98}(y,2)}$	1.4, 1.6
τ_{He}^*	4
Avge neutron wall loading (MWm^{-2})	3.5
Peak neutron wall loading (MWm^{-2})	4.6

Table 1: Base-line parameters for the STPP.

combination of bootstrap and diamagnetic current. Having fixed β_N and I_{rod}/I_p within their limits, the toroidal field is determined (the fusion power required fixes the plasma stored energy), and hence the plasma current. To minimise the requirements for an external current drive system (be it neutral beam injection or RF current drive), we work at a relatively low plasma density which is somewhat below the Greenwald density and significantly short of the optimum density for fusion power if auxiliary current drive were not an issue. The remaining parameter is the confinement time: when the device parameters are chosen according to these criteria, the confinement time is an output and a test against expected confinement scalings provides a test of the overall consistency of the assumed plasma parameters. Our base-line case is consistent with the best confinement data from MAST and NSTX, being $\sim 50\%$ above the predictions of the international scaling laws, IPB98(y,1) and IPB98(y,2) [4], derived using confinement data from conventional tokamaks.

3. Current drive

A spherical tokamak power plant must operate without a central solenoid as there is no room to accommodate the shielding which would be required to protect the insulation; therefore all the current has to be provided by some other means. During the steady state burning phase, current must be provided non-inductively and this drives one to a design with a high bootstrap current driven fraction. This has a large influence on the design, so it is worthwhile considering the main parameters which influence bootstrap current. Integrating across the plasma cross-section, the bootstrap current can be written as:

$$I_{bs} = 2\pi \int d\psi \frac{\langle \mathbf{J}_{bs} \cdot \mathbf{B} \rangle}{\langle B^2 \rangle} q = 2\pi \int d\psi \frac{C_{bs} f q}{\langle B^2 \rangle} \frac{dp}{d\psi} \quad (1)$$

where angled brackets denote flux surface average, p is the plasma pressure, q is the safety factor, $f = RB_\phi$, ψ is the poloidal flux, R is the major radius, B_ϕ is the toroidal component of the

basis for their design [3]. The size is chosen so that the thermal and neutron wall loadings are tolerable, giving lifetimes of the mid-plane blanket modules commensurate with the maintenance targets. We shall see that a high pressure-driven (bootstrap and diamagnetic) current fraction is needed to meet the steady state requirement, and this drives one to high β_N , high I_{rod}/I_p and high elongation, κ . Here I_p is the plasma current, I_{rod} is the current down the centre column, and β_N is β expressed as a percentage normalised to $I_p(\text{MA})/a(\text{m})B_0(\text{T})$. These all have limits: β_N is limited by ideal MHD stability, I_{rod}/I_p is limited by cost of electricity (due to Ohmic power dissipation in the centre column) and κ is limited by vertical instability. Nevertheless, working within these limits we find that more than 90% of the current can be provided by a

magnetic field and C_{bs} is a coefficient which depends on the aspect ratio and ratio of temperature to density gradients of the plasma species. To derive an approximate scaling for the bootstrap current fraction, we can replace C_{bs} and q by some weighted average across the plasma, and write

$$\frac{I_{bs}}{I_p} \sim \frac{C_{bs} RBqp}{I_p \langle B^2 \rangle} \sim \beta_N \frac{I_{rod}}{I_p} h(\kappa) \quad (2)$$

where $h(\kappa)$ is an increasing function of κ , arising mainly from q . Numerically one typically finds $h(\kappa)$ is approximately linear, but it depends on the details of the current profile. One of the key features of the ST is its high natural elongation, and Eq (2) shows that it is essential to exploit this capability to gain full advantage of the ST configuration. This is the main reason for our choice, $\kappa=3.2$ leading to a total of 28.7MA of pressure-driven current.

The bootstrap current has the property that it vanishes at the magnetic axis, and therefore such a large pressure-driven current fraction inevitably leads one to a hollow current profile. Here we note another important difference between the conventional tokamak and the ST: a monotonic q profile can be maintained in an ST even if the current profile is hollow. It may turn out that a non-monotonic q -profile has beneficial properties (such as generation of internal transport barriers) that outweigh the challenges associated with MHD stability, but for the present we assume that a monotonic q -profile is the more desirable, and design our current drive system to provide this. In Fig 1 we show profiles for (a) the total current density, (b) the required externally driven current profile and (c) the resulting q -profile.

From Fig 1, we see that auxiliary current drive must be provided in two regions: 0.14MA on axis and 2.17MA at the plasma edge. A study of the neutral beam current drive efficiency for this equilibrium indicates that this scheme is a suitable candidate for both regions. The edge current could be provided by 6 or 7 inclined 80keV beams with a total power of 40MW, while the current drive on axis would require a 500keV, 20MW beam. RF schemes also provide useful current drive options. For example, although electron cyclotron current drive (ECCD) proves to be inefficient at the plasma edge, it is an option for the core current drive. An interesting complication arises here because on the outboard side the poloidal and toroidal magnetic fields become comparable, and lead to an increase of the total magnetic field with R there. Thus, there is parasitic absorption of the waves as they pass through the edge region. Nevertheless, for high harmonic heating in the frequency range ~ 130 -150GHz, accessibility is acceptable, and results in ~ 15 MW required for the on-axis current drive (using 4th harmonic damping). Although the power requirements are similar to NBI, ECCD has the advantages that small ports would be required, freeing up more space for tritium breeding, and the windows avoid the need for an extended containment envelope. An alternative scheme that we are also exploring is to use conversion of electron cyclotron waves into electron Bernstein waves, which do not have a high-density cut-off, and are expected to give good current drive

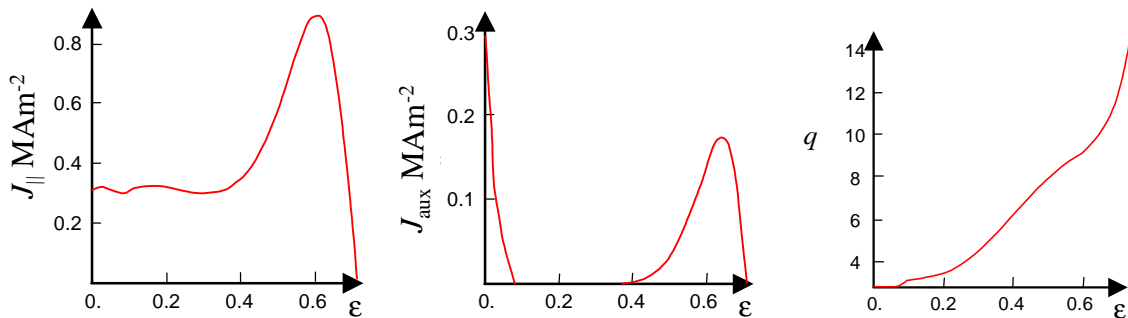


Figure 1: The flux surface average of the total parallel current profile, the driven current profile and the q profile as a function of the inverse aspect ratio, ϵ , of the flux surfaces.

efficiency. Indeed, preliminary calculations indicate that if the waves can penetrate through to the core, then a very high efficiency $\sim 0.1 \text{AW}^{-1}$ can be achieved on axis. This is very promising, but a scenario to avoid the premature damping still needs to be identified. Turning now to the edge current drive, it is natural to consider the efficiency of lower hybrid, LH, waves. As expected, calculations indicate that LHCD is efficient for edge current drive and a power in the region $\sim 20\text{-}30\text{MW}$ would be required, which is again similar to that calculated for the neutral beam system. The disadvantage with LHCD is the antenna which needs to be positioned close to the plasma and the design of this, to withstand the hostile environment, is a major challenge.

4. MHD stability issues

The β -limiting ideal MHD stability issues for these types of plasma have been addressed elsewhere [5,6], so we shall not go into details here. We have constrained our pressure and current profiles so that the plasma is in the second stability regime to $n=\infty$ ballooning modes across the full minor radius (n is the toroidal mode number). It was shown in ref [6] that external kink modes ($n=1,2$) can be stabilised by placing the wall sufficiently close to the plasma (within $\sim 25\%$ of the minor radius). Internal MHD modes (eg infernal modes) were found to be stable for the equilibrium studied there, but a full analysis of the robustness of this result to variations in profiles (eg pressure and q) needs further work. Other issues which remain to be addressed include the stability of the intermediate n ideal MHD modes, resistive wall modes and neoclassical tearing modes. One point to note about neoclassical tearing modes is that STPP operates at high q , and low order rational surfaces are excluded from the plasma (see Fig 1). This eliminates the most dangerous tearing modes, and may prove to be a key advantage of the ST.

Another important issue to address is the vertical stability, particularly as we are at a much higher elongation than one would consider in a conventional tokamak. Nevertheless there are two features of our design which allow us to go to such high elongations: tighter aspect ratio and lower internal inductance both tend to increase the natural elongation. To quantify our vertical stability it is necessary to develop a solution to the free boundary equilibrium. The engineering design allows for three pairs of poloidal field, PF, coils, and the chosen double null operation leads to an up-down symmetry about the mid-plane (see Fig 2). The desired plasma shape can be achieved with the following PF coil currents: 3.885MA in the divertor coil, PF1, -8.0MA in PF2 and -4.375MA in PF3. The resulting equilibrium is very close to marginal stability, but is not quite naturally stable. In the presence of the vacuum vessel we find very small growth rates, $\sim 100\text{s}^{-1}$ and a stability parameter $f_s=3.5$ (f_s is the ratio of stabilising to destabilising force gradients [7]). This should be easy to compensate with a feedback coil.

5. Alpha-particle orbits and ripple losses

There are two important features of α -particle orbits in STPP (see Fig 3): (1) the banana width is comparable to the Larmor radius and (2) the orbit width is reduced at the outboard mid-

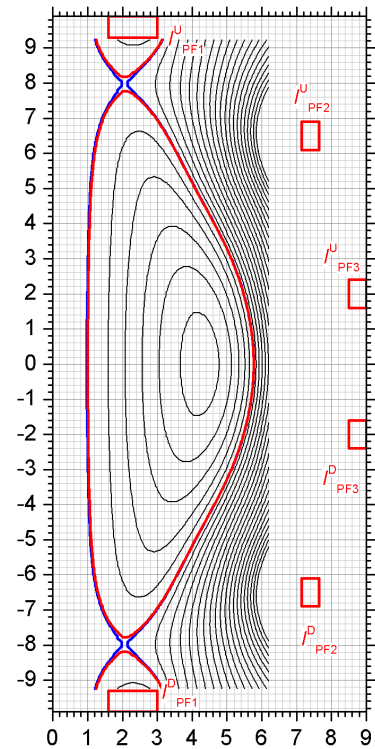


Figure 2: Poloidal cross-section of the free boundary equilibrium reconstruction showing the positions of the PF coils.

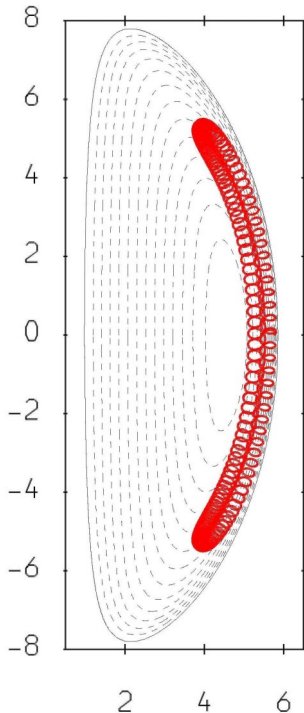


Figure 3: Full orbit of a trapped 3.5MeV α -particle in STPP.

We have also performed 1-D transport simulations with the ASTRA code [9], coupled to a full 2-D equilibrium code, SCENE [10]. Figure 4 shows the results for a case with very similar parameters to those of Table 1. The density profile was fixed, and the line averaged density evolved according to a pre-set time-dependence. We start at time $t=0$ with a low density, low current ‘seed’ plasma, and then ramp the current (artificially fast in this case) and density to steady operating values. The temperature and current profiles evolve according to the transport equations. For the temperature diffusivities, we adopt the canonical profiles transport model (CPTM) [11] and enhance the constant ‘background’ diffusivity so that the confinement cannot exceed 1.4 times the IPB98(y,1) law; this is more pessimistic than the CPTM, which has weak power degradation. From the time traces shown in Fig 4, it can be seen that the plasma does indeed settle down to a steady state, with a fusion power close to 3GW. The final electron and ion temperatures are very similar over much of the profile, the exception being deep in the plasma core where the ion temperature reaches 34keV and the electron temperature 38keV.

We turn now to one of the key issues for any fusion device: the exhaust. There is a large uncertainty in the peak power density that has to be handled, due to uncertainties in the scrape-off layer

plane due to increasing poloidal magnetic field there (see Section 3). The first effect means that a full orbit code is required to study α -particle losses, for which we have developed the new code, CUEBIT [8]. The orbit pinching effect helps to improve energetic α -particle confinement. We follow a large number of 3.5MeV α -particles, distributed radially according to the fusion power density. The velocity distribution is taken to be isotropic on the outboard mid-plane (for simplicity), so that our predictions for lost particles are somewhat pessimistic. If we neglect the toroidal field ripple, the losses are low, $\sim 2.4\%$. The number of toroidal field coils ($N=16$) has been chosen to ensure that the ripple magnitude is less than 1% across the entire plasma to keep the ripple induced losses low. This could be further reduced by the use of magnetic plates if required, but initial estimates using CUEBIT indicate that the total fraction of lost α -particles is tolerable ($\sim 4-5\%$).

6. Transport and Exhaust

The design we have described so far is based on 0-D scaling laws for the transport. For example, we find that an enhanced confinement a factor 1.4 above the IPB98(y,1) scaling law is required. Data from MAST and NSTX do seem to be broadly consistent with these scaling laws, and the best discharges have a confinement comparable with our assumptions.

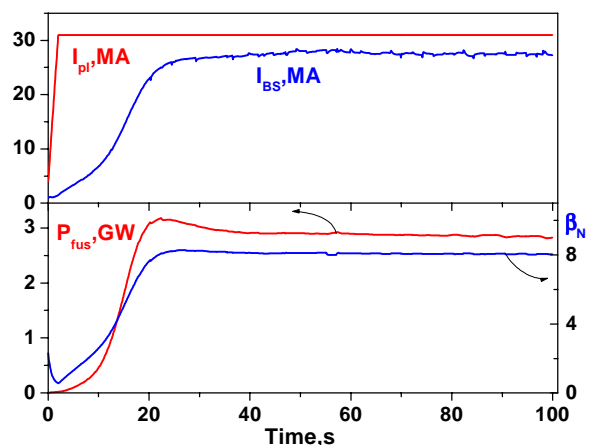


Figure 4: Prescribed evolution of plasma current, and calculated evolution of bootstrap current, β_N and fusion power.

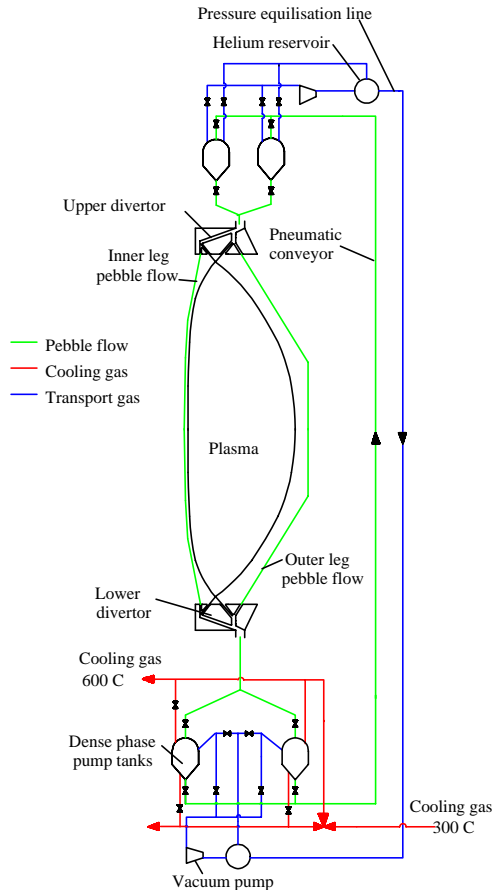


Figure 5: Layout for the cascading pebble divertor concept

leads to SOL widths at the target plates of 27.7mm and 3.3mm, respectively. Taking the outboard leg to be at a major radius of 3.5m and the inboard to be at 1.2m and angling the outer (inner) divertor plate so that the SOL strikes it at an angle of 10° (5°) leads to a total wetted area of 3.5m^2 on the outboard side and only 0.29m^2 on the inboard side. Thus, double null operation would lead to power densities on the inboard and outboard legs of $\sim 26\text{MWm}^{-2}$ and $\sim 40\text{MWm}^{-2}$, respectively, for a steady, L-mode like discharge. If we were to consider H-mode operation, with ELMs, then the ELMs would have to be very small (much less than 1% of the stored energy) to have any chance of being tolerable. In addition, the ratio of the outboard to inboard power during the inter-ELM periods is likely to be lower in H-mode (in MAST H-modes only $\sim 80\%$ of the power flows to the outboard side).

Clearly, unless the strike angles can be reduced significantly, novel divertor schemes need to be developed, and one which we are considering is a scheme based on a cascading curtain of pebbles, made of SiC. The layout of the divertor system is shown in Fig 5. The pebbles, 2-3mm in diameter, enter the top first and are immediately split into two flows: one for the inner divertor legs and one for the outer. They accelerate under free-fall before passing through the first divertor leg, after which they are collected and flow (more slowly) through ducts behind the shield on the inboard side and channels between the blanket modules on the outboard side. They then accelerate again under free-fall before passing through the lower leg and being collected in one of two chambers, until it is half-full. The flow is then switched to the second chamber while the pebbles in the first are cooled by filling the chamber with He at 5bar and fluidising: this rapidly cools the pebbles from 1200°C down to 600°C . The high grade heat is usefully employed as part of the steam cycle. The cooled pebbles can now be transferred by a

(SOL) thickness and, if we operate in ELMy H-mode, the size of the ELMs. In order to get some idea of the kinds of powers involved, we extrapolate recent measurements from MAST, as follows. First, 95% of the power in MAST flows to the outer divertor leg during either L-mode or ELMs, which in MAST are predominantly Type III to date. There are a number of mechanisms which could contribute to this: a large surface area on the outboard side, a ballooning nature to the turbulence and a large Shafranov shift. These mechanisms are also likely to hold for the STPP plasma, and therefore we take 95% of the power to flow to the outboard side. An estimate of the SOL width is required, and as an example we use a model in which the heat-flux across the SOL is dominated by resistive ballooning mode turbulence; this model provides one of the best fits to MAST data. This predicts a width of 7.9mm on the outboard mid-plane and 2.2mm on the inboard midplane for STPP; both of these exceed the thermal ion Larmor radius. Let us assume that 50% of the power can be radiated, so that only $\sim 300\text{MW}$ of α -power has to be handled by the divertor: 285MW to the outboard leg and 15MW to the inboard leg for an L mode plasma. Allowing for a realistic flux expansion factor on the outboard side of 3.5 and 1.5 on the inboard side

pneumatic conveyor into the top chamber until it is full, after which it is isolated from the conveyor, and the tank can be evacuated to repeat the cycle. This avoids the need for complex mechanisms to transport the pebbles and offers high reliability. Detailed calculations have been performed for the temperature rise and the stresses the pebbles must endure, and the system can indeed accommodate high power loads. To illustrate this we outline here a more simplistic calculation. Taking M to be the mass flow rate of the pebbles, C_p to be the specific heat capacity of the pebble material and Δ to be the tolerable temperature rise, the power that can be handled is $P=MC_p\Delta$. Taking SiC balls of radius 1.5mm, these can tolerate temperatures in excess of 1500°C, so we assume they enter the upper divertor at 600°C and leave the lower at 1200°C, so that $\Delta=600\text{K}$. The value of C_p for SiC increases strongly with temperature, but at 900°C is 1200Jkg⁻¹K⁻¹ so that a mass flow rate of ~400kg s⁻¹ would be required to handle the power. Further work is needed to demonstrate and optimise issues like the cooling rate, the properties of the pebble flow through pipes, etc, but this does seem to provide a possible solution to a challenging problem, which could also be applied to other fusion concepts.

7. Engineering design

In this section we provide a brief overview of the extensive engineering design that has been developed [1,2]. The toroidal magnetic field (TF) is produced by a water-cooled, solid copper centre rod with 16 copper return limbs. A steel shield (also water-cooled) around the centre rod captures 245MW of the neutron power load, while the remaining 88MW is absorbed by the copper rod. The rod, which weighs a total of 650 tonnes, could be formed from an assembly of 30 tapered, spiral copper plates wrapped around a central tube; these plates would have grooves machined into them to form the coolant channels.

Turning to the first wall, this is envisaged to be of martensitic steel construction, designed to handle a maximum thermal heat flux of 1MWm⁻² and can accommodate the peak neutron wall loading of 4.6MWm⁻². The first wall is an integral part of the blanket, and both are designed to be replaced every 2 years as we describe below. A pebble bed technology is employed for the blanket, with lithium silicate chosen for the tritium-generating material. Thus, the design consists of layers of beryllium multiplier and silicate, separated by helium-cooled steel plates;

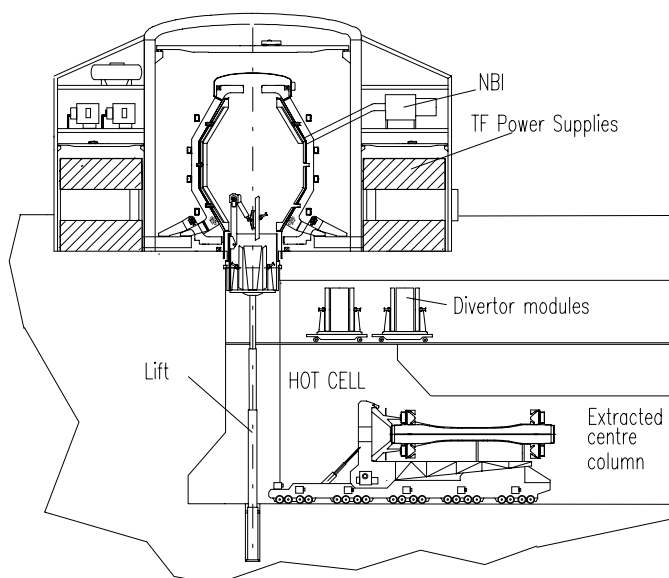


Figure 6: Cross-section of STPP layout during maintenance: centre column removed ready for replacement; the remote arm is just lowering one of the lower blanket modules into its transporter.

the same helium also provides the coolant for the first wall. Each layer is compartmentalised by steel corrugations which allows the Li₆ enrichment to be graded and so provide a more even power density profile without compromising the tritium breeding ratio, which is ~1.1.

Three pairs of PF coils are positioned outside the vessel and TF limbs. The smaller radius, divertor coils, are normal conducting copper while the base-line design for the other two pairs of PF coils is conventional superconductor (cryogenic, copper PF coils may also be an option to simplify the design at the expense of reduced efficiency).

The fusion energy released in the

plant is recovered as heat, and whilst most of this is at high temperature, a significant fraction (21%) is at lower temperature (70-200°C). To optimise the efficiency of the power plant, careful consideration has gone into the design of the power cycle, which takes account of this broad spectrum of heat quality. The steam generator uses the high-grade heat from the blanket, first wall and divertor pebbles, whilst the lower grade heat is used to preheat feed water for the steam generator. The end result is that the steam cycle operates at a thermal efficiency of 43%, providing 1.75GW of shaft output power. Approximately 30% of the output electrical power is fed back into the plant to drive the main electrical sub-systems.

On the engineering side, one of the most attractive features of STPP is the simplicity of the design, offering the possibility of easy maintenance. Indeed, ease of maintenance is essential, as the centre column and equatorial blanket modules would need to be changed and refurbished every 2 years. This could coincide with statutory inspections of the steam plant. Each centre column can then be re-used up to 3 times by replacing the steel shield and divertor components with new ones. Maintenance of the internal components is achieved by constructing a cell below the load assembly (Fig 6). The old centre column can then be lowered and taken away for refurbishment. This leaves a large open space inside the vessel for a remote control arm to operate, removing those first wall and blanket structures that need replacement (those above and below the equatorial plane must be replaced every 4 years). The new centre column can then be installed, ready to resume operation. A highly desired feature of fusion power plants is ease of maintenance, and the ST does appear to be attractive in this respect.

8. Summary

In summary, we have continued to iterate our design for a fusion power plant based on the ST concept. The overall design remains feasible, but there are challenges: in particular the exhaust handling issue. We have presented a possible solution to this problem, and we will continue to explore and test the feasibility of the cascading pebbles design. The plasma physics questions continue to be addressed and it appears, at least theoretically, that a self-consistent set of plasma parameters does exist for an ignited, steady state ST plasma. Of course uncertainties remain, but with further experimental and theoretical ST research, together with burning plasma data from a device such as ITER, the ST is well-placed to provide an option for the fusion power plants following ITER.

Acknowledgement This work was supported by EURATOM and the UK Dept. of Trade & Industry.

References

- [1] VOSS G. M., et al, Fusion Engineering and Design **51-52** (2000) 309
- [2] VOSS G. M., et al, Proceedings of ISFNT, San Diego (2002)
- [3] NAJMABADI F., et al, Proc. of Fusion Energy Conference, Yokohama (1998) FTP/08
- [4] ITER Physics Basis Document, Nucl Fusion **39** (1999) 2204
- [5] AKERS R. A., et al, Nucl Fusion **40** (2000) 1223, and references therein
- [6] ROBINSON D C, et al, Proc. of Fusion Energy Conference, Yokohama (1998) FTP/05
- [7] LEUER J. A., Fusion Technology **15** (1989) 489
- [8] HAMILTON, B., et al., Proc. 10th European Solar Physics Meeting, Prague (2002)
- [9] PEREVERZEV G.V. and YUSHMANOV P.N., IPP Report 5/98 (2002)
- [10] WILSON H. R., UKAEA Fusion Report UKAEA FUS 271 (1994)
- [11] DNESTROVSKIY Yu. N., et al, Plasma Phys Rep **26** (2000) 579